Interplay of Light Antenna and Excitation "Energy Reservoir" Effects in a Bichromophoric System Based on Ruthenium–Polypyridine and Pyrene Units Linked by a Long and Flexible Poly(ethylene glycol) Chain[†]

Angeles Farrán Morales,[‡] Gianluca Accorsi,[‡] Nicola Armaroli,[‡] Francesco Barigelletti,*,[‡] Simon J. A. Pope,[§] and Michael D. Ward*,[§]

Istituto per la Sintesi Organica e Fotoreattività (ISOF-CNR), Via P. Gobetti 101, I-40129 Bologna, Italy, and School of Chemistry, University of Bristol, Cantock's Close, Bristol BS8 ITS, U.K.

Steady-state and time-resolved spectroscopic properties of bichromophoric species containing $[Ru(bpy)_3]^{2+}$ and pyrene (pyr) units linked together by flexible poly(ethylene glycol) chains of variable length, $[Ru(bpy)_2(bpy-pyr)](PF_6)_2$ (**1**) and $[Ru(bpy)_2(bpy-O6-pyr)](PF_6)_2$ (**2**), have been investigated in acetonitrile solvent. The complexes were designed with the aim of examining the intercomponent energy-transfer processes taking place after light absorption at the two chromophores and the influence of the distance separation between them; in the case of complex **2**, the linking chain in the extended conformation is as long as 21 Å. Direct excitation of the pyrene unit ($\lambda_{exc} = 410$ nm) results in singlet-to-singlet energy transfer (an antenna effect) to the Ru-based component, ^{1}pyr $\rightarrow$ ^{1}MLCT, which we analyze in terms of the Förster mechanism taking place with unit efficiency. Analysis of the time-resolved pyrene fluorescence reveals that the actual center-to-center distance separation (d_{cc}) between the photoactive centers changes according to a Gaussian distribution, with an average $d_{cc} = 13.6$ Å (distribution width, $a = 2.8$ Å) and 12 Å ($a = 10.2$ Å), for **1** and **2**, respectively; this is ascribed to folding of the poly(ethylene glycol) linking chain. In O_2-free solvent at room temperature, after population of the ^{1}MLCT level (which takes place either because of direct excitation by using $\lambda_{exc} > 355$ nm or via the "antenna" effect) and subsequent intersystem crossing localized at the Ru center, ^{1}MLCT $\rightarrow$ ^{3}MLCT, a triplet–triplet thermal equilibration is established which involves the physically separated centers, ^{3}MLCT $\leftrightarrow$ ^{3}pyr, with $K_{eq} = 11$ (the energy gap between the two levels is 480 cm^{-1}, as determined from luminescence data obtained at 77 K). As a consequence of this equilibrium, the ^{3}MLCT luminescence lifetime becomes $\tau_{Ru} \sim 9$ μs both in **1** and **2**, i.e., 1 order of magnitude longer than for the unsubstituted $[Ru(bpy)_3]^{2+}$ luminophore. In air-equilibrated solvent, diffusional quenching by O_2 effectively depletes the ^{3}pyr level and only the forward ^{3}MLCT $\rightarrow$ ^{3}pyr energy transfer step is observed with $k_{en} = 4 \times 10^8$ and 2×10^8 s^{-1} for **1** and **2**, respectively. As briefly discussed, reasons for the high rate constants observed for the various triplet–triplet steps may be traced back to the folding properties of the linking chains.

Introduction

The study of the excited-state dynamics between components of supramolecular species designed for light energy conversion and storage is of uppermost importance.[1–6]

Transition metal complexes based on d^6 or d^{10} metal centers and polyimine ligands are capable of visible light absorption and formation of luminescent metal-to-ligand charge-transfer

* To whom correspondence should be addressed. E-mail: franz@frac.bo.cnr.it (F.B.).
[†] Dedicated to Prof. Vincenzo Balzani, in recognition of his contribution to the development of inorganic photochemistry.
[‡] Istituto ISOF-CNR, Bologna.
[§] University of Bristol.

(1) Wasielewski, M. R. *Chem. Rev.* **1992**, *92*, 435.
(2) Lehn, J.-M. *Supramolecular Chemistry*; VCH: Weinheim, Germany, 1995.
(3) de Silva, A. P.; Gunaratne, H. Q. N.; Gunnlaugsson, T.; Huxley, A. J. M.; McCoy, C. P.; Rademacher, J. T.; Rice, T. E. *Chem. Rev.* **1997**, *97*, 1515.
(4) Balzani, V.; Campagna, S.; Denti, G.; Juris, A.; Serroni, S.; Venturi, M. *Acc. Chem. Res.* **1998**, *31*, 26.
(5) Gust, D.; Moore, T. A.; Moore, A. L. *Acc. Chem. Res.* **2001**, *34*, 40.
(6) Stoddart, J. F. *Acc. Chem. Res.* **2001**, *34*, 410.

triplet levels (^{3}MLCT); as such, they have proved very useful as photoactive centers within an impressive number of supermolecules.[7−13]

A major effort concerned with the design and usage of these complexes within energy conversion schemes has been to gain extensive control (or tuning) of properties such as the profile of the optical absorption spectrum, the energy content of the lowest lying electronic level (the one temporarily storing the energy captured after light absorption), and its luminescence intensity and lifetime;[12−16] the last property is of obvious relevance for the design of schemes where metal-complexed units play as energy or electron donors.

Recently, an interesting approach dealing with complexes of the Ru- or Os-based polypyridine families has been that of equipping them with one or more covalently linked aromatic chromophores;[17−32] for a case involving a Pt-based chromophore, see ref 33. As long as a convenient energy match between lowest lying levels is realized, the organic moiety can play the role of "energy reservoir" toward the M-based luminophore.[17,22,26] In particular, for the well-known [Ru(bpy)$_3$]$^{2+}$ species, pyrene (pyr) has proved to be an effective reservoir. In this case, additive effects on the lifetime of the [Ru(bpy)$_3$]$^{2+}$-based luminescence have been observed upon the use of 3[30] or 1-to-6 appended pyrenes.[34] This outcome is basically due to the establishment of a thermal equilibrium between the triplet levels centered on the two types of covalently joined chromophores, ^{3}[Ru-(bpy)$_3$]$^{2+}$ and ^{3}pyr.

The other relevant process in the excited-state dynamics of these coupled systems regards a possible antenna function[30] played by the appended pyrene unit. This occurs by the following sequence: (a) direct light absorption at pyrene; (b) formation of its singlet excited level, ^{1}pyr; (c) disposal of its excitation energy in favor of the accessible levels of the other component, ^{1}[Ru(bpy)$_3$]$^{2+}$ and ^{3}[Ru(bpy)$_3$]$^{2+}$. Both processes—thermal equilibration and antenna effects—are expected to be affected by the nature and spatial extension of the connectors (or bridging ligands, BLs). Until now, typical BLs have usually been relatively short saturated or unsaturated units, with varying degree of rigidity.[17−27,29−31,34] In this work, we wanted to address the role of a large distance separation between the photoactive [Ru(bpy)$_3$]$^{2+}$ and pyrene chromophores by using a flexible poly(ethylene glycol) BL,[35] which features a fully extended end-to-end distance of about 21 Å. To this end, we have prepared the reference bpy-pyr ligand and complexes **1** and **2**, illustrated in Chart 1. From the spectroscopic results obtained in O$_2$-free and air-equilibrated solutions, we see that (a) the ^{1}pyr → ^{1}[Ru-(bpy)$_3$]$^{2+}$ energy-transfer process most likely takes place with unit efficiency both in **1** and **2** (a detailed investigation of this step provides a picture of the conformer distribution exhibited by BL) and that (b) thermal equilibration between the ^{3}[Ru(bpy)$_3$]$^{2+}$ and ^{3}pyr excited levels is reached for the cases both of **1** and **2,** even if for the larger complex **2** some degree of spatial and electronic separation might be expected solely on the basis of its geometric features (see Chart 1).

Experimental Section

Syntheses. General Details. Organic starting materials [1-(hydroxymethyl)pyrene, pentakis(ethylene glycol), 2,2′-bipyridine] were purchased from Aldrich and used as received. Hydrated ruthenium trichloride was kindly loaned by Johnson Mathey plc. The compounds 1-(bromomethyl)pyrene,[36] 5-(bromomethyl)-2,2′-bipyridine,[37] and [RuCl$_2$(bpy)$_2$]·2H$_2$O[38] were prepared according to the literature procedures.

bpy-pyr. 1-(Hydroxymethyl)pyrene (0.186 g, 8.03 × 10^{-4} mol) was dissolved in dry THF (30 mL) under dinitrogen, and excess KH (1.2 equiv) was added. This mixture was allowed to stir for about 30 min after which 5-(bromomethyl)-2,2′-bipyridine (0.2 g, 8.03 × 10^{-4} mol) was added and the mixture heated to reflux for 6 h. After cooling, the reaction was quenched by addition of water, concentrated in vacuo, and the residue extracted with CH$_2$Cl$_2$, which

(7) Ballardini, R.; Balzani, V.; Credi, A.; Gandolfi, M. T.; Venturi, M. *Acc. Chem. Res.* **2001**, *34*, 445.
(8) Armaroli, N.; Balzani, V.; Collin, J. P.; Gavina, P.; Sauvage, J. P.; Ventura, B. *J. Am. Chem. Soc.* **1999**, *121*, 4397.
(9) Balzani, V., Ed. *Electron Transfer in Chemistry*; Wiley-VCH: Weinheim, Germany, 2001; Vol. 3.
(10) Balzani, V.; Scandola, F. *Supramolecular Photochemistry*; Ellis Horwood: New York, 1991.
(11) Bignozzi, C. A.; Schoonover, J. R.; Scandola, F. *Mol. Level Artif. Photosynth. Mater.* **1997**, *44*, 1.
(12) Armaroli, N. *Chem. Soc. Rev.* **2001**, *30*, 113.
(13) McMillin, D. R.; McNett, K. M. *Chem. Rev.* **1998**, *98*, 1201.
(14) Kober, E. M.; Caspar, J. V.; Lumpkin, R. S.; Meyer, T. J. *J. Phys. Chem.* **1986**, *90*, 3722.
(15) Juris, A.; Balzani, V.; Barigelletti, F.; Campagna, S.; Belser, P.; von Zelewsky, A. *Coord. Chem. Rev.* **1988**, *84*, 85.
(16) Dixon, I. M.; Collin, J. P.; Sauvage, J. P.; Flamigni, L.; Encinas, S.; Barigelletti, F. *Chem. Soc. Rev.* **2000**, *29*, 385.
(17) Ford, W. E.; Rodgers, M. A. J. *J. Phys. Chem.* **1992**, *96*, 2917.
(18) Wilson, G. J.; Sasse, W. H. F.; Mau, A. W. H. *Chem. Phys. Lett.* **1996**, *250*, 583.
(19) Kneas, K. A.; Xu, W. Y.; Demas, J. N.; DeGraff, B. A. *Appl. Spectrosc.* **1997**, *51*, 1346.
(20) Simon, J. A.; Curry, S. L.; Schmehl, R. H.; Schatz, T. R.; Piotrowiak, P.; Jin, X. Q.; Thummel, R. P. *J. Am. Chem. Soc.* **1997**, *119*, 11012.
(21) Wilson, G. J.; Launikonis, A.; Sasse, W. H. F.; Mau, A. W. H. *J. Phys. Chem. A* **1997**, *101*, 4860.
(22) Wilson, G. J.; Launikonis, A.; Sasse, W. H. F.; Mau, A. W. H. *J. Phys. Chem. A* **1998**, *102*, 5150.
(23) Harriman, A.; Hissler, M.; Ziessel, R. *Phys. Chem. Chem. Phys.* **1999**, *1*, 4203.
(24) Harriman, A.; Hissler, M.; Khatyr, A.; Ziessel, R. *Chem. Commun.* **1999**, 735.
(25) Hissler, M.; Harriman, A.; Khatyr, A.; Ziessel, R. *Chem.—Eur. J.* **1999**, *5*, 3366.
(26) Tyson, D. S.; Castellano, F. N. *J. Phys. Chem. A* **1999**, *103*, 10955.
(27) Bonnefous, C.; Chouai, A.; Thummel, R. P. *Inorg. Chem.* **2001**, *40*, 5851.
(28) Juris, A.; Prodi, L. *New J. Chem.* **2001**, *25*, 1132.
(29) Sohna, J. E. S.; Carrier, V.; Fages, F.; Amouyal, E. *Inorg. Chem.* **2001**, *40*, 6061.
(30) Tyson, D. S.; Henbest, K. B.; Bialecki, J.; Castellano, F. N. *J. Phys. Chem. A* **2001**, *105*, 8154.
(31) Del Guerzo, A.; Leroy, S.; Fages, F.; Schmehl, R. H. *Inorg. Chem.* **2002**, *41*, 359.
(32) Tyson, D. S.; Bignozzi, C. A.; Castellano, F. N. *J. Am. Chem. Soc.* **2002**, *124*, 4562.
(33) Michalec, J. F.; Bejune, S. A.; Cuttell, D. G.; Summerton, G. C.; Gertenbach, J. A.; Field, J. S.; Haines, R. J.; McMillin, D. R. *Inorg. Chem.* **2001**, *40*, 2193.
(34) McClenaghan, N. D.; Barigelletti, F.; Maubert, B.; Campagna, S. *Chem. Commun.* **2002**, 602.
(35) Pope, S. J. A.; Rice, C. R.; Ward, M. D.; Morales, A. F.; Accorsi, G.; Armaroli, N.; Barigelletti, F. *J. Chem. Soc., Dalton Trans.* **2001**, 2228.
(36) Okamoto, H.; Arai, T.; Sakuragi, H.; Tokumaru, K. *Bull. Chem. Soc. Jpn.* **1990**, *63*, 2881.
(37) Eaves, J. G.; Munro, H. S.; Parker, D. *J. Chem. Soc., Chem. Commun.* **1985**, 684.
(38) Sullivan, B. P.; Salmon, D. J.; Meyer, T. J. *Inorg. Chem.* **1978**, *17*, 3334.

A Bichromophoric System

Chart 1. Formulas of the Investigated Compounds

$[Ru(bpy)_3]^{2+}$

bpy-pyr

1

2
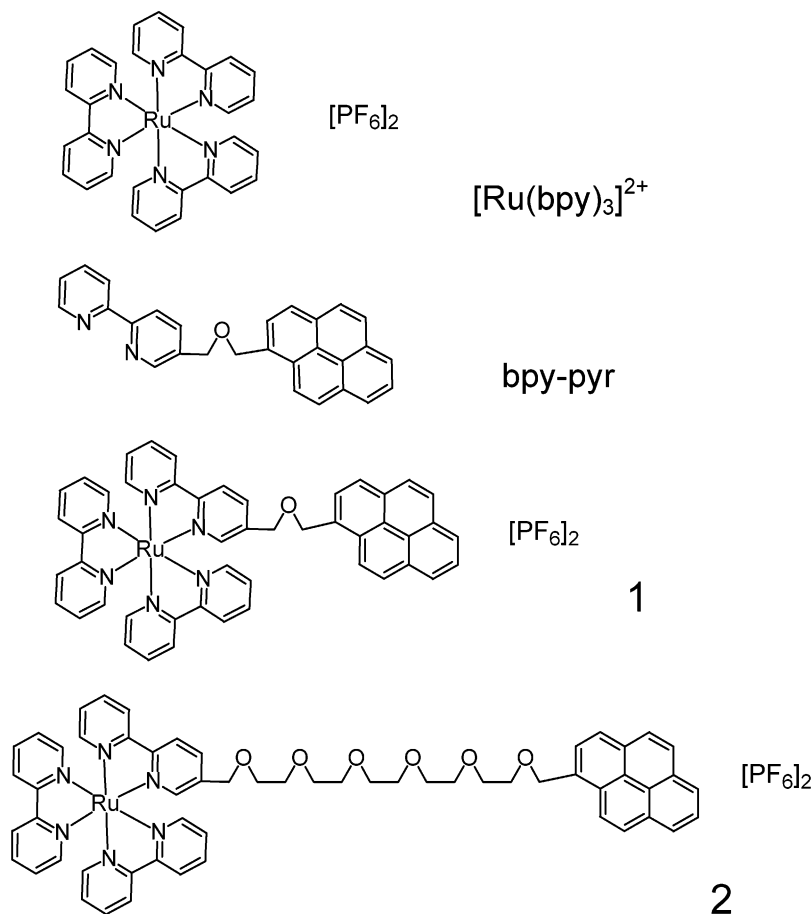
was evaporated off. The brown residue was introduced to a silica column. Initially The column was initially eluted with CH_2Cl_2, to remove fast-eluting impurities including a very bright yellow species, and then with CH_2Cl_2/MeOH (19:1). The product was collected as a yellow-brown oil which solidifies when dry, (yield 0.251 g, 78%). Anal. Calcd for $C_{28}H_{20}N_2O$: C, 80.8; H, 4.8; N, 6.7. Found: C, 80.9; H, 5.1; N, 7.1. EIMS (CH_2Cl_2): m/z 400 (M^+), 215 ($M - OCH_2bpy)^+$. ^1H NMR (270 MHz, $CDCl_3$): δ 8.68 (2H, m, bpy $H^6/H^{6'}$), 8.38 (2H, m, bpy $H^3/H^{3'}$), 8.25–7.95 (9H, m, pyrene), 7.82 (2H, m, bpy $H^4/H^{4'}$), 7.30 (1H, m, bpy $H^{5'}$), 5.31 (2H, s, bpyCH$_2$O), 4.71 (2H, s, pyrene–CH$_2$O).

Pyrene-O6H. Pentakis(ethylene glycol) (0.2 g, 8.4×10^{-4} mol) was dissolved in dry THF (30 mL) to which was added NaH (5×10^{-3} mol, 6 equiv). A solution of 1-(bromomethyl)pyrene (0.248 g, 8.4×10^{-4} mol) in THF (10 mL) was added dropwise, and the mixture was refluxed under dinitrogen for 24 h. After workup (see above) the brown residue was introduced to a silica column. The column was initially eluted with CH_2Cl_2, to remove fast-running impurities, and then with CH_2Cl_2/MeOH (19:1). The product was collected as a brown oil (yield 0.205 g, 54%). EIMS (CH_2Cl_2): $m/z = 452$, $[M]^+$.

**bpy-O6-pyr.** To a solution of pyrene-O6H (0.25 g, 5.53×10^{-4} mol) in dry THF (30 mL) under dinitrogen was added NaH (3.3×10^{-3} mol, 6 equiv). To this was added dropwise a solution of 5-(bromomethyl)-2,2′-bipyridine (0.138 g, 5.53×10^{-4} mol) in dry THF (10 mL), and the mixture was then refluxed for 24 h. After workup and chromatography (as above for bpy-pyr), the product was collected as a brown oil (yield 0.233 g, 68%). Calcd for $C_{38}H_{40}N_2O_6$: C, 73.6; H, 6.5; N, 4.5. Found: C, 73.5; H, 6.8; N, 4.7. EIMS (CH_2Cl_2): $m/z = 644$, $(M + Na)^+$. ^1H NMR (270 MHz,

$CDCl_3$): δ 8.66 (2H, m, bpy $H^6/H^{6'}$), 8.38 (2H, m, bpy $H^3/H^{3'}$) 8.25–7.95 (9H, m, pyrene), 7.79 (2H, m, bpy $H^4/H^{4'}$), 7.29 (1H, m, bpy $H^{5'}$), 5.27 (2H, s, bpyCH$_2$O), 4.59 (2H, s, pyrene-CH$_2$O), 3.8–3.6 (20H, m, OCH$_2$CH$_2$O).

[Ru(bpy)$_2$(bpy-pyr)](PF$_6$)$_2$ (1). A mixture of bpy-pyr (0.06 g, 1.5×10^{-4} mol) and [RuCl$_2$(bpy)$_2$]·2H$_2$O (0.078 g, 1.5×10^{-4} mol) in EtOH (30 mL) under N$_2$ was refluxed for 8 h. The solvent was removed and the residue purified using column chromatography on silica, eluting with MeCN–H$_2$O–KNO$_3$(aq, sat) (14:2:1). Very small fractions were collected to eliminate contamination of the desired product with [Ru(bpy)$_3$]$^{2+}$. Once the main red band was collected, the addition of NH$_4$PF$_6$(aq), reduction in volume, and extraction into CH$_3$CN/CHCl$_3$ gave the product (yield 0.113 g, 68%). Calcd for $C_{48}H_{36}N_6OP_2F_{12}Ru$: C, 52.2; H, 3.3; N, 7.6. Found: C, 51.8, H, 3.1; N, 8.0. FAB MS (3-NOBA): $m/z = 960$ $(M - PF_6)^+$, 814 $(M - 2PF_6)^+$.

[Ru(bpy)$_2$(bpy-O6-pyr)](PF$_6$)$_2$ (2). This was prepared from bpy-O6-pyr (0.05 g, 8.06×10^{-5} mol) and [RuCl$_2$(bipy)$_2$]·2H$_2$O (0.042 g, 8.06×10^{-5} mol) in exactly the same manner used for preparation of [Ru(bpy)$_2$(bpy-O1-pyr)](PF$_6$)$_2$ (above). The product was obtained as an orange solid (yield 0.068 g, 64%) and recrystallized from chloroform/hexane. Calcd for $C_{58}H_{56}O_6N_6P_2F_{12}Ru$·2CHCl$_3$: C, 46.1; H, 3.7; N, 5.4. Found: C, 45.6; H, 3.7; N, 5.4. FAB MS (3-NOBA): $m/z = 1346$ $(M + Na)^+$, 1202 $(M - PF_6 + Na)^+$, 1179 $(M - PF_6)^+$, 1034 $(M - 2PF_6)^+$.

Spectroscopy. Absorption spectra of dilute acetonitrile solutions (2×10^{-5} M) of the investigated complexes were obtained with a Perkin-Elmer Lambda 5 spectrophotometer. Luminescence spectra were obtained with a Spex Fluorolog II spectrofluorometer, equipped with a Hamamatsu R928 phototube. Sample solutions

Scheme 1[a]
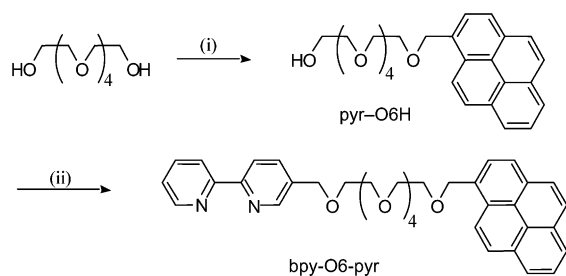
[a] Key: (i) 1-(bromomethyl)pyrene, NaH, THF; (ii) 5-(bromomethyl)-2,2′-bipyridine, NaH, THF.

were freeze−pump−thaw vacuum-degassed or air-equilibrated with absorbance values ≤0.15 at the indicated excitation wavelength. While uncorrected band maxima are used throughout the text, corrected spectra were employed for the determination of the luminescence quantum yields. The correction procedure takes care of the wavelength-dependent phototube response, either by using a software provided by the firm or by employing a calibrated 45 W quartz-halogen tungsten filament lamp (Optronic Laboratories) as a standard. From the area of the luminescence spectra on an energy scale (cm^{-1}), we obtained luminescence quantum yields Φ for the samples with reference to [Ru(bpy)$_3$]$^{2+}$ as a standard (r, Φ_r = 0.028 in air-equilibrated water)[39] and by using eq 1, where Abs and n are absorbance values and refractive index of the solvent, respectively. Band maxima and relative luminescence intensities were affected by an uncertainty of 2 nm and 20%, respectively. Low-temperature measurements of the luminescence properties were performed in capillary tubes immersed in liquid nitrogen within homemade quartz dewars. Luminescence lifetimes were obtained using an IBH single-photon counting spectrometer equipped with a nitrogen-filled thyratron gated lamp (λ_{exc} 337 or 358 nm). The uncertainty in the lifetime values is within 8%.

$$\frac{\Phi}{\Phi_r} = \frac{(Abs_r)n^2(area)}{(Abs)n_r^2(area)_r} \qquad (1)$$

Transient absorption spectra were obtained by using as light source the second harmonic (532 nm) of a Nd:YAG laser (JK Lasers) with 20 ns pulse and 1−2 mJ of energy/pulse. Triplet lifetimes were obtained by averaging five different decays recorded around the maximum of the absorption peak at 420 nm. Details on the flash-photolysis system are reported elsewhere.[40]

Modeling of excited-state equilibria and energy-transfer calculations was performed with the help of Matlab 5.0 by MathWorks, Natick, MA.

Results and Discussion

Syntheses. The ligands bpy-pyr and bpy-O6-pyr were prepared as outlined in Scheme 1. Synthesis of bpy-pyr was by straightforward alkylation of 1-(hydroxymethyl)pyrene with 5-(bromomethyl)-2,2′-bipyridine using NaH/THF. Synthesis of bpy-O6-pyr required stepwise functionalization of each end of a pentakis(ethylene glycol) unit in turn, first with 1-(bromomethyl)pyrene and second with with 5-(bromo-methyl)-2,2′-bipyridine. Attachment of [Ru(bpy)$_2$]$^{2+}$ units to the bpy sites of these ligands to give complexes **1** and **2** was effected in the usual manner, and the formulations of
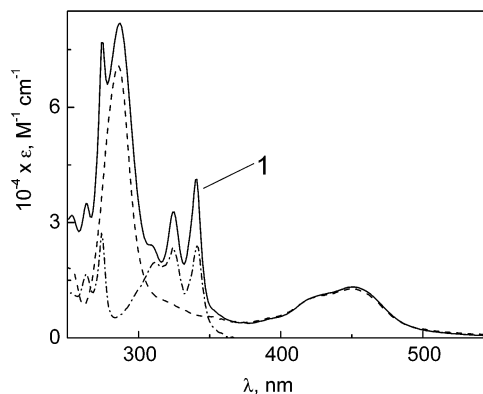
(39) Nakamaru, K. *Bull. Chem. Soc. Jpn.* **1982**, *55*, 2967.
(40) Flamigni, L. *J. Phys. Chem.* **1992**, *96*, 3331.

Figure 1. Room-temperature absorption spectra of complexes **1** (full line) and [Ru(bpy)$_3$]$^{2+}$ (dashed line) and of the ligand bpy-pyr (dash−point line).

the resulting complexes were confirmed by FAB mass spectrometry and elemental analysis. For complex **2** the long glycol chain meant that the complex retained traces of solvent tenaciously; the elemental analysis was consistent with the presence of ca. two molecules of chloroform.

Absorption and Luminescence Spectra. Figure 1 shows the absorption spectra for **1**, bpy-pyr, and [Ru(bpy)$_3$]$^{2+}$ in acetonitrile (the spectrum of **2** overlaps with **1** and is not shown). Comparison of the absorption profiles displayed in this figure allows the following assignments. For complex **1**, the band maximum at 452 nm originates from MLCT (Ru → bpy) transitions and the features in the 280−290 nm spectral portion are of LC (mostly bpy centered) nature; the absorption characteristics in the region 320−340 nm are identified as being of pyrene origin and ascribed to popula-tion of the ^{1}pyr excited state. For **1** (and likewise for **2**), close inspection of the absorption spectra of Figure 1 indicates that absorption results from additive properties of scarcely interacting Ru-based and pyrene chromophores. This is in line with expectations on the basis of the fact that the poly(ethylene glycol) unit linking the chromophores in **1** (and **2**) provides both a spatial and electronic separation of the photoactive units.[35] From the absorption properties, one sees that, for **1** (and **2**), use of $\lambda_{exc} \geq 355$ nm results in selective excitation of the Ru-based component; on the other hand, use of $\lambda_{exc} = 340$ nm leads to predominant (but not selective) excitation of the pyrene component.

The room-temperature luminescence properties of **1** and **2** in acetonitrile solutions are illustrated by data collected in Table 1; for comparison purposes, luminescence results for [Ru(bpy)$_3$]$^{2+}$ are also listed. Luminescence spectra for **1** and bpy-pyr, as obtained by using λ_{exc} 340, are shown in Figure 2. The luminescence spectrum of **1** (and of **2**, not shown in the figure) exhibits features in the higher energy portion of the spectrum to be ascribed to the fluorescence properties of the pyrene unit (for bpy-pyr in degassed acetonitrile, λ_{em} = 380 nm, Φ_f = 0.42, τ_f = 90 ns; a detailed analysis of the quenching of the pyrene-based fluorescence in **1** and **2** is provided below). For **1**, **2**, and [Ru(bpy)$_3$]$^{2+}$, the lumines-cence spectra (or spectral portions) at $\lambda \geq 500$ nm exhibit overlapping profiles, with the band maxima peaking at 608 nm; in a vacuum-degassed samples, the luminescence quantum yields obtained by using λ_{exc} = 450 nm gave Φ =

A Bichromophoric System

Table 1. Parameters from Luminescence Experiments[a]

	λ_{em},[b] nm	Φ[b]	τ_1,[c] μs	τ_2,[c] ns	k_f,[d] s^{-1}	K_{eq}[e]
O$_2$-free						
1	608	0.096	8.8	2.9	3 × 10^8	11
2	608	0.117	10.0	5.9	2 × 10^8	11
[Ru(bpy)$_3$]$^{2+}$	608	0.086	0.90			
air-equilibrated						
1	608	1.7 × 10^{-3}	0.21	2.4	4 × 10^8	
2	608	2.4 × 10^{-3}	0.19	4.5	2 × 10^8	
[Ru(bpy)$_3$]$^{2+}$	608	0.02	0.22			

[a] Acetonitrile solvent. [b] Band maximum and luminescence quantum yield; unless otherwise stated, λ_{exc} = 450 nm. [c] λ_{exc} = 358 nm, λ_{em} = 608 nm; single or dual exponential analysis, $I(t) = b_1 \exp(-t/\tau_1)$ or $I(t) = b_1 \exp(-t/\tau_1) + b_2 \exp(-t/\tau_2)$, respectively. [d] $k_{en} = 1/\tau_2 - 1/\tau_1$. [e] $K_{eq} = k_f/k_b$ and is evaluated from equilibrium modeling as $\alpha/(1 - \alpha)$; see text.
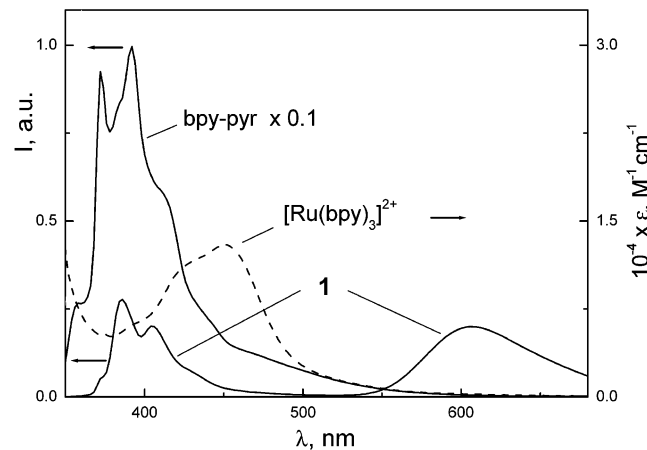

Figure 2. Luminescence spectra of complex **1** and ligand bpy-pyr as obtained in O$_2$-free acetonitrile, λ_{exc} = 340 nm. The absorption spectrum of [Ru(bpy)$_3$]$^{2+}$ (dashed line) is also shown.
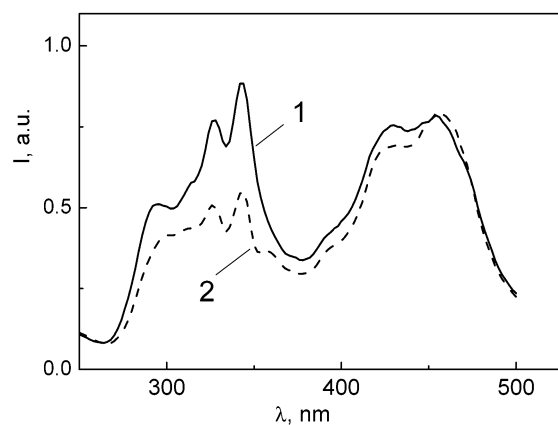

Figure 3. Uncorrected excitation spectra of **1** (full line) and **2** (dashed line) in degassed acetonitrile solution with λ_{em} = 608 nm.

0.096, 0.117, and 0.086, respectively (Table 1, as an average, $\Phi_{av} \sim 0.1$). These results are consistent with a ^{3}MLCT nature for the lowest lying emission of **1** and **2**, as typical for Ru−polypyridine luminophores.[15] In air-equilibrated samples, the luminescence quantum yields were $\Phi = 1.7 \times 10^{-3}$ and 2.4 × 10^{-3}, for **1** and **2**, respectively, i.e., 1 order of magnitude smaller than for [Ru(bpy)$_3$]$^{2+}$ ($\Phi = 0.02$; see Table 1).

Figure 3 displays the room-temperature (uncorrected) excitation spectra of **1** and **2**, as observed at λ_{em} = 608 nm in degassed acetonitrile. The spectra are characterized by features typical of the Ru-based chromophore (spectral
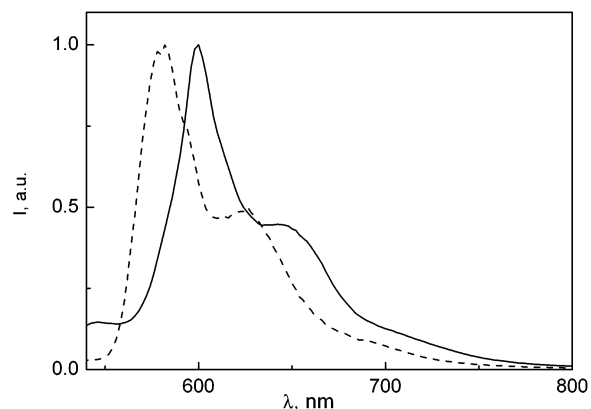

Figure 4. Luminescence spectra obtained at 77 K for **1** (full line) and [Ru(bpy)$_3$]$^{2+}$ (dashed line) with λ_{exc} = 450 nm.

regions around 450 and 280 nm) and of the pyrene unit (320−340 nm range), consistent with the absorption profile; see Figure 1. These results indicate that the observed ^{3}MLCT luminescence in **1** and **2** receives contributions from the ^{1}pyr level, in addition to ^{1}LC and ^{1}MLCT levels of Ru-based origin. In principle, this may happen because of three competing intercomponent processes, viz. (i) a singlet−singlet energy transfer, ^{1}pyr → ^{1}MLCT (followed by an intersystem crossing step localized at the Ru center, ^{1}MLCT → ^{3}MLCT), (ii) a direct intersystem crossing, ^{1}pyr → ^{3}MLCT, and (iii) an intersystem crossing localized at pyrene, ^{1}pyr → ^{3}pyr, followed by thermal redistribution (at room temperature; see below) between the close-lying Ru- and pyr-centered triplet levels.

Figure 4 shows the luminescence spectra obtained at 77 K for [Ru(bpy)$_3$]$^{2+}$[41] and **1** in frozen acetonitrile solvent, by using λ_{ex} = 450 nm (the spectrum observed for **2** overlaps with that of **1** and is not shown). The luminescence lifetimes were 4.9 μs and 80 ms, respectively (70 and 700 ms for **2** and bpy-pyr, respectively). Comparison with literature results[15,17,30] allows the assignment of the luminescence spectra of Figure 4 to ^{3}MLCT (for [Ru(bpy)$_3$]$^{2+}$) and ^{3}py (for **1**) excited levels, peaking at 585 and 602 nm, respectively. Thus, for the case of **1** (and of **2**) at 77 K, excitation into the Ru-based chromophore results in phosphorescence emission at the pyrene unit. This is in contrast with the behavior observed at room temperature, where the lowest lying registered luminescence is of Ru-based ^{3}MLCT nature; this difference must be ascribed to a temperature effect. Actually, the energy gap between the ^{3}MLCT and ^{3}pyr levels, as estimated from the luminescence band maxima of Figure 4, is 480 cm^{-1}. On this basis, the thermal redistribution between ^{3}pyr and ^{3}MLCT levels is expected to lead to a [^{3}pyr]:[^{3}MLCT] ratio ca. 3 orders of magnitude larger at 77 K than at room temperature.

Results from measurements of absorption, luminescence, and excitation spectra are summarized in Scheme 2. Here, we have indicated the energy layout of the relevant excited levels of **1** and **2** which are populated after light absorption.

(41) Exactly overlapping spectra were obtained by using [Ru(bpy)$_3$]$^{2+}$ and a [Ru(bpy)$_3$]$^{2+}$ complex with one ligand functionalized at the 5 position with a poly(ethylene glycol) chain; see ref 35.

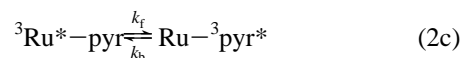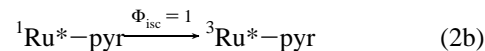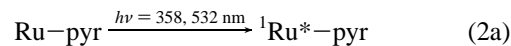**Scheme 2.** Energy Levels of the Relevant Excited States
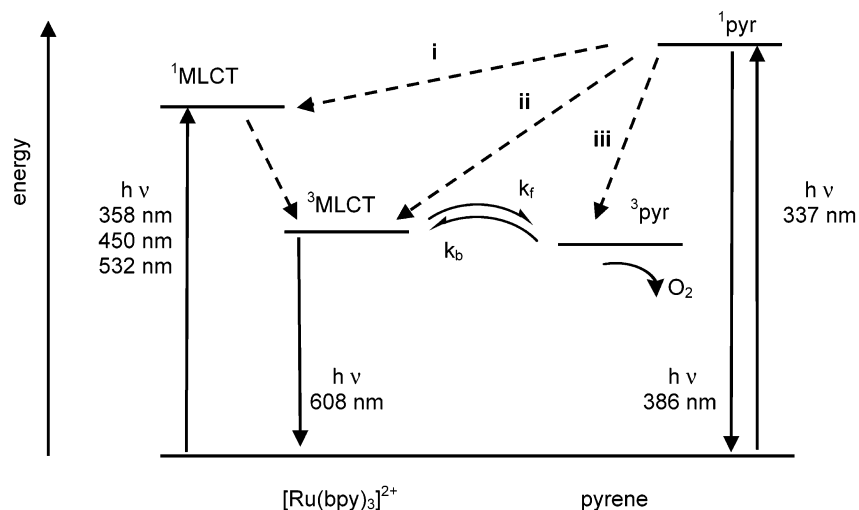
The dashed arrows within Scheme 2 provide hints about the connection between the various levels. Intermolecular diffusional quenching of the ^{3}pyr level by oxygen is expected to be effective, given its long lifetime, $\tau(^3\text{pyr}) = 150\ \mu\text{s}$,[42] and the concerned step is also indicated in the scheme.

Time-Resolved Spectroscopy and Oxygen Effect. The time-resolved properties of the excited states of the investigated complexes were examined at room temperature by luminescence and transient absorption spectroscopy by using both vacuum-degassed and air-equilibrated samples; results are discussed separately in the following. Parameters drawn from luminescence experiments are collected in Table 1.

Kinetics in O$_2$-Free Solution. The luminescence decay times, as detected at 608 nm after 358 nm excitation of
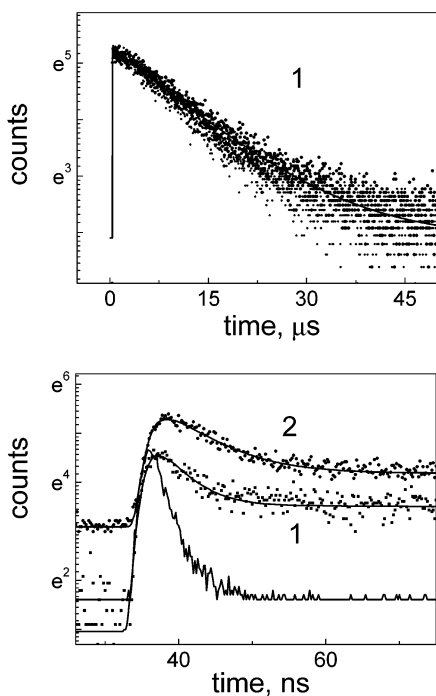

Figure 5. Top: Decay of the luminescence intensity of **1** (in degassed acetonitrile) on a long time scale. Bottom: Decay of the luminescence intensity of **1** and **2** on a short time scale. (In degassed acetonitrile, the flash profile is also shown.) In all cases, $\lambda_{\text{exc}} = 358$ nm, $\lambda_{\text{em}} = 608$ nm, and full lines come from numerical fitting procedures; see text.

degassed samples and analyzed according to a single-exponential decay law, $I(t) = b_1 \exp(-t/\tau_1)$, provided $\tau_1 = 0.9$, 8.8, and 10 μs for [Ru(bpy)$_3$]$^{2+}$, **1**, and **2**, respectively (see Table 1 and Figure 5, top). Results from parallel transient absorption experiments are displayed in Figure 6 for the case of **2**; λ_{exc} was 532 nm. Comparison of the transient absorption profile with results from bpy-pyr and cases from the literature allowed assignment of the absorption to the lowest lying ^{3}pyr level $(T_1 \rightarrow T_n)$.[17] This was found to decay according to a single-exponential law with $\tau = 9.6\ \mu$s; see inset of Figure 6. Analogous experiments on **1** provided a quite similar series of time-resolved spectra which decayed with $\tau = 9.0\ \mu$s. Therefore, for both **1** and **2**, selective excitation ($\lambda_{\text{exc}} = 358$ and 532 nm; see Scheme 2) of the [Ru(bpy)$_3$]$^{2+}$ moiety leads to a Ru-based luminescence and a pyr-based transient absorption which decay with a common lifetime $\tau \sim 9\ \mu$s. These results are consistent with the establishment of a thermal equilibrium involving the triplet levels centered on the [Ru(bpy)$_3$]$^{2+}$ and pyrene moieties of **1** and **2** (eq 2c), following light absorption (eq 2a) and fast intersystem-crossing steps (isc, eq 2b).[15,43]

$$\text{Ru-pyr} \xrightarrow{h\nu = 358,\ 532\ \text{nm}} {}^1\text{Ru*-pyr} \qquad (2a)$$

$$^1\text{Ru*-pyr} \xrightarrow{\Phi_{\text{isc}} = 1} {}^3\text{Ru*-pyr} \qquad (2b)$$

$$^3\text{Ru*-pyr} \underset{k_b}{\overset{k_f}{\rightleftharpoons}} \text{Ru-}^3\text{pyr*} \qquad (2c)$$

As a consequence, the luminescence quantum yield for degassed samples of **1**, **2**, and [Ru(bpy)$_3$]$^{2+}$ is practically the same ($\Phi \sim 0.1$), while the Ru-based luminescence lifetime is 1 order of magnitude longer in **1** and **2** than in [Ru(bpy)$_3$]$^{2+}$; see Table 1. This is precisely the "reservoir effect" previously observed in other cases were the Ru- and pyr based units were linked via short bridging units, both of saturated and unsaturated type.[17,18,21–26,30] For our cases we

(42) Murov, S. L.; Carmichael, I.; Hug, G. L. *Handbook of Photochemistry*; Marcel Dekker: New York, 1993.
(43) Damrauer, N. H.; Cerullo, G.; Yeh, A.; Boussie, T. R.; Shank, C. V.; McCusker, J. K. *Science* **1997**, *275*, 54.
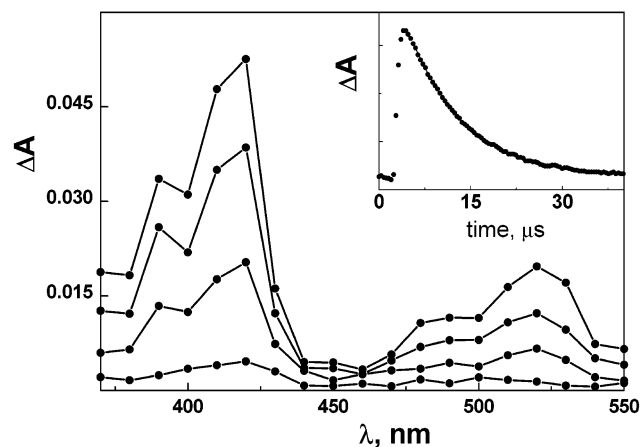
Figure 6. Transient absorption results recorded in degassed acetonitrile for **2** with λ_{exc} = 532 nm. The spectra were obtained at delays of 3, 6, 9, and 20 μs after the laser pulse; the inset shows the absorbance decay observed at λ = 420 nm.

obtain such a "reservoir effect" even when employing relatively long bridges; for **2**, a full extension of the linking chain would place the photoactive units at a center-to-center separation >21 Å.

Close inspection of the faster portion of the luminescence decay traces as observed at 608 nm, Figure 5, bottom, revealed a more complex behavior, and analysis performed according to a dual exponential law, $I(t) = b_1 \exp(-t/\tau_1) + b_2 \exp(-t/\tau_2)$, provided τ_2 = 2.9 and 5.9 ns for **1** and **2**, respectively. We interpret these findings by suggesting that the shorter-lived component detected from luminescence experiments (τ_2; see Table 1) is related to the Ru → pyr forward step of eq 2c, $k_f = 1/\tau_2$, where $K_{eq} = k_f/k_b$ (see Scheme 2); this issue is further treated in the following.[44]

Kinetics in Air-Equilibrated Solution. The same time-resolved experiments illustrated above were performed in air-equilibrated samples. In the presence of O_2, the $T_1 \rightarrow T_n$ pyrene absorption in **1** and **2** (see Figure 6 for the O_2-free case of **2**) is no more observed; this is due to complete quenching of the of the ^{3}pyr level by dissolved O_2. Interestingly, the luminescence results obtained for the air-equilibrated case and by monitoring the band at 608 nm (see Table 1) indicate that the forward ^{3}Ru → ^{3}pyr step takes place. In fact, the Ru-based luminescence intensity in the presence of O_2 is ca. 1 order of magnitude lower for both **1** and **2** with respect the reference complex, $[Ru(bpy)_3]^{2+}$ (Φ = 0.02), consistent with quenching of the Ru-based luminescence in the bichromophoric molecules. Furthermore, for both **1** and **2**, the luminescence decay is described in terms of a dual exponential law, with a minor long-lived component ($\tau_1 \approx 0.2$ μs, likely due to a residual unquenched Ru-based luminescence) and a short-lived component (τ_2 = 2.4 and 4.5 ns for **1** and **2**, respectively, practically identical to that exhibited in degassed samples; see above). This is interpreted by suggesting that, for both **1** and **2** in air-equilibrated

(44) The dual exponential analysis should be accomplished by employing distribution functions for the faster decay; the averaged values for the shorter lifetime we obtain are possibly to be ascribed to intramolecular quenching involving conformers where the two chromophores are at closer distance than the average distance.

conditions, forward ^{3}Ru → ^{3}pyr energy transfer takes place while back-transfer (described by k_f and k_b of eq 2c, respectively, Scheme 2) does not. Use of the results provided $k_{en} = k_f \sim 4 \times 10^8$ and 2×10^8 s^{-1} for **1** and **2**, respectively (Table 1).

Pyrene as a Light Antenna. As seen above, Figure 2 compares the fluorescence profile of bpy-pyr (i.e., of its ^{1}pyr level) with that of complex **1**, which features both a high-energy ^{1}pyr-based residual contribution and a lower energy ^{3}MLCT luminescence. In the figure is also shown the absorption spectrum of $[Ru(bpy)_3]^{2+}$ which is identical to that of the Ru-based unit of **1**, Figure 1. As one can see, there is a favorable spectral overlap between the emission profile due to the ^{1}pyr level and the absorption profile of the $[Ru(bpy)_3]^{2+}$ unit. With reference to Scheme 2, this suggests that ^{1}pyr → $^1[Ru(bpy)_3]^{2+}$ energy transfer, path i, may effectively compete against paths ii and iii. Actually, for pyrene in polar solvent, the last step is estimated to take place with $k_{isc} \approx 2 \times 10^6$ s^{-1},[42] and owing to the distance between the involved sites, step ii is likely to be even slower. Thus, it is interesting to gain a picture of the energy disposal process after absorption of light in the 330−340 nm region (i.e., at the pyrene unit; see Scheme 2). To this aim, we have first calculated parameters for the dipole−dipole energy transfer (Förster mechanism)[45] involving the ^{1}pyr donor level and the $^1[Ru(bpy)_3]^{2+}$ acceptor state, i.e., path i of Scheme 2. Subsequently, we show how useful mechanistic details can be drawn by analyzing the time-resolved features of the ^{1}pyr fluorescence exhibited by complexes **1** and **2**.

Singlet−Singlet py → $[Ru(bpy)_3]^{2+}$ Energy Transfer. Regarding the dipole−dipole mechanism connecting the singlet levels of pyr and $[Ru(bpy)_3]^{2+}$, evaluation of the spectral overlap J_F (eq 3) between the fluorescence profile of the donor (^{1}pyr) and the absorption profile of $[Ru(bpy)_3]^{2+}$ (Figure 2) allows estimates of the critical transfer radius (i.e., of the distance at which the energy transfer efficiency is 50%), R_0 (Å), eq 4.[45]

$$ J_F = \frac{\int F(\bar{\nu})\epsilon(\bar{\nu})/\bar{\nu}^4 \, d\bar{\nu}}{\int F(\bar{\nu})} \tag{3} $$

$$ R_0 = 9.79 \times 10^{-3} (K^2 n^{-4} \Phi J_F)^{1/6} \tag{4} $$

In the above eqs, $F(\bar{\nu})$ and $\epsilon(\bar{\nu})$ are fluorescence and absorption profiles on an energy scale (cm^{-1}), K^2 is a geometric factor (taken as 2/3 for statistical reasons), Φ and τ are the fluorescence quantum yield and lifetime for the donor (taking bpy-pyr as a reference, these were 0.42 and 90 ns, respectively), and n is the refractive index of the solvent. Results were as follows: $J_F = 1.8 \times 10^{-14}$ cm^3 M^{-1}; R_0 = 29 Å; $k_{en}^F \geq 1 \times 10^7$ s^{-1} for $d_{cc} \leq R_0$. For both **1** and **2** complexes, the two units are at a distance separation d_{cc} $\ll R_0$ (for the larger complex **2**, the fully extended linking chain is as long as 21 Å). On this basis, path i of Scheme 2 is predicted to be the predominant path for deactivation of

(45) Förster, T. *Discuss. Faraday Soc.* **1959**, *27*, 7.

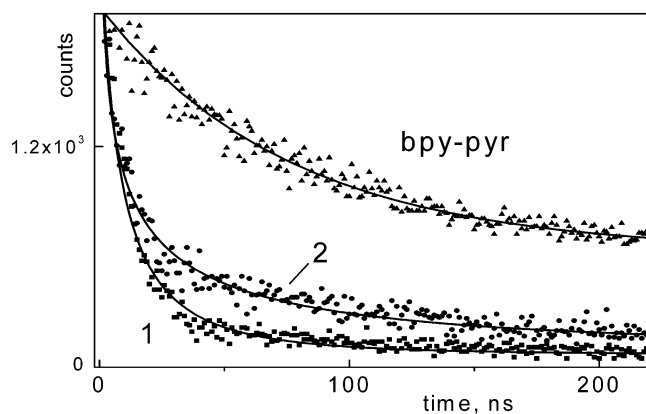**Figure 7.** Time-resolved decay of the ^{1}pyr fluorescence of bpy-pyr, **1**, and **2**, as detected at 410 nm in degassed acetonitrile.
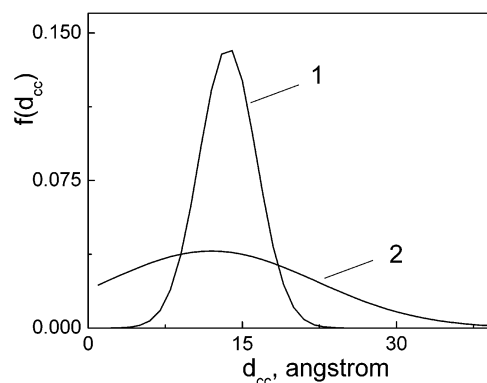

Figure 8. Gaussian distribution of the Ru- and pyrene-based intercomponent distance, d_{cc}, in complexes **1** and **2** as estimated from analysis of the decay of the ^{1}pyr fluorescence.

the ^{1}pyr state given that, as seen above, the competing steps ii and iii take place with $k \leq 2 \times 10^6$ s^{-1}.

Distribution of Intercomponent Distances. The folding properties of poly(ethylene glycol) chains are known.[35] Because of these properties, it is foreseeable that the two interacting chromophores of **1** and **2** are closer each other than what can be predicted on the basis of a linear extension of the connecting chain. We have addressed this issue by analyzing the ^{1}pyr fluorescence decay as monitored at 410 nm (Figure 2). Decay profiles are plotted in Figure 7; data points and fitting curves are displayed. These were obtained according a nonlinear iterative analysis and following an approach described by Lakowicz,[46] which takes into account a Gaussian distribution, $f(d_{cc})$, for the distance between donor and acceptor units:

$$f(d_{cc}) = \frac{1}{a\sqrt{2\pi}} \exp\left[-0.5\left(\frac{d_{cc} - \mu}{a}\right)^2\right] \qquad (5)$$

In this equation μ is the most likely distance and a represents the width of the distribution. On this basis, the fluorescence decay of the ^{1}pyr level undergoing intramolecular quenching by the ^{1}[Ru(bpy)$_3$]$^{2+}$ level (see Scheme 2) can be described by[46]

$$I(t) = A\int_0^\infty f(d_{cc}) \exp\left[-\frac{t}{\tau_d}\left(\frac{R_0}{d_{cc}}\right)^6\right] \mathrm{d}d_{cc} \qquad (6)$$

where A is a preexponential factor, R_0 is the critical transfer radius, and τ_d is the lifetime of the unquenched ^{1}pyr state. Analysis of the $I(t)$ dependences shown in Figure 7 gave $\mu = 13.6$ and $a = 2.8$ Å for **1** and $\mu = 12.0$ and $a = 10.2$ Å for **2** (for the critical transfer radius R_0, 21 and 22 Å were obtained, respectively, which appear underestimated with respect to the result provided by use of eqs 3 and 4). The Gaussian distribution for d_{cc} in the two cases is compared in Figure 8. At the evaluated values for the distance separation, μ, the Förster rate constants is calculated $k_{en}^F \geq 10^9$ s^{-1}. These findings strongly support a unit efficiency for step i in Scheme 2.

Pyrene as an Excitation Energy Reservoir. At room temperature and in degassed solvent, the "reservoir effect" of pyrene toward a spatially close, luminescent [Ru(bpy)$_3$]$^{2+}$ unit is well established.[17-31,34] This results from the fact that (a) the ^{3}pyr level is more stable than the ^{3}MLCT level by few hundreds of cm^{-1}, (b) the lifetime of ^{3}pyr is far longer ($\tau_p \sim 10^2$ μs)[42] than that of ^{3}[Ru(bpy)$_3$]$^{2+}$, $\tau_{Ru} = 0.9$ μs, and (c) the interconverting rate constants for the equilibrium depicted in eq 2c and Scheme 2 are larger than the involved decay constants, k_f, $k_b \gg (\tau_{Ru})^{-1}$, $(\tau_p)^{-1}$.[47,48] As a consequence, thermal redistribution between the two levels results in observable luminescence properties (band maximum, luminescence profile, and luminescence quantum yield) typical of the ^{3}MLCT state but with a luminescence lifetime, τ_{eq}, which benefits from the thermal redistribution between the two levels:

$$\tau_{eq}^{-1} = \alpha\tau_p^{-1} + (1 - \alpha)\tau_{Ru}^{-1} \qquad (7)$$

Here α is the fraction of **1** or **2** with populated ^{3}pyr states and $1 - \alpha$ is the fraction with populated ^{3}MLCT levels, so that $K_{eq} = \alpha/(1 - \alpha)$. From the luminescence band maxima of Figure 4, the energy gap between the ^{3}MLCT and ^{3}pyr levels is estimated as 480 cm^{-1}. Evaluation of the room-temperature equilibrium indicated in Scheme 2, O$_2$-free case, provided $\alpha = 0.92$, $K_{eq} = 11$, and an equilibrated lifetime $\tau_{eq} = 9$ μs, in agreement with the time-resolved results both from luminescence and transient absorption experiments (Figures 5 and 6 and Table 1); the input parameters employed for modeling the equilibrium were $\tau_{Ru} = 0.9$ μs, $\tau_p = 150$ μs,[30] k_f as listed in Table 1, and $k_b = k_f/K_{eq}$.[49] It is to be recalled that in air-equilibrated acetonitrile, the ^{3}pyr level is depleted by O$_2$-quenching, Table 1. Actually, in this solvent [O$_2$] = 1.9×10^{-3} and the diffusion-controlled rate constant is $k_{diff} = 1.9 \times 10^{10}$ M^{-1} s^{-1}, which results in $k_q^{O_2} = 3.6 \times 10^7$ s^{-1}. Thus, $k_q^{O_2}$ is much larger than $(\tau_p)^{-1}$ and slightly larger than k_b, which explains why use of excitation at 532

(46) Lakowicz, J. R. *Principles of Fluorescence spectroscopy*; Plenum: New York, 1999.

(47) The fact that derived k_f and k_b constants are triplet−triplet energy-transfer rate constants is consistent with the interacting units being at distance close to "contact", as required by an "exchange"-type mechanisms; see ref 48.
(48) Dexter, D. L. *J. Chem. Phys.* **1952**, *21*, 836.
(49) Modeling of excited-state equilibria was performed with the help of Matlab 5.0 by MathWorks.

nm allowed observation of the ^{3}MLCT $\rightarrow$ ^{3}pyr forward step but not of the backward step.

Conclusions

For complexes **1** and **2**, two photoactive components, [Ru-(bpy)$_3$]$^{2+}$ and pyrene, are tethered by poly(ethylene glycol) chains of different lengths. The various energy-transfer paths consequent to light absorption localized at the two components, both in degassed and air-equilibrated acetonitrile, have been monitored. For both the **1** and **2** cases, whatever the spatial localization of the excitation energy, this is finally funneled to the Ru-based triplet level, ^{3}MLCT, the only luminescent level at room temperature. In particular, according to a so-called antenna effect, the excitation energy stored at ^{1}pyr (consequent to light absorption at this component) is exclusively conveyed to the ^{1}[Ru(bpy)$_3$]$^{2+}$ level {the direct precursor of ^{3}[Ru(bpy)$_3$]$^{2+}$} because of a Förster-type step[45]—a critical transfer radius $R_0 = 29$ Å is evaluated for this intrinsically long-distance transfer. From the triplet Ru-based level, forward energy transfer to the lower lying ^{3}pyr level takes place. This short-range triplet—

triplet transfer is subject to double-electron exchange restrictions[48,50] and requires electronic mediation via "super-exchange" paths.[51−53] The occurrence of this step is likely related to the folding properties of the linking chains because the two chromophores are found at an average center-to-center separation of 13.6 and 12 Å (cases of **1** and **2**, respectively; for the latter, the linking chain in a fully extended configuration is as long as 21 Å). On this basis, the triplet—triplet transfer might be allowed because of through space interactions, possibly enhanced by some electronic mediation from interposed fragments of the linker. Once populated, the ^{3}pyr level is either involved in back-transfer to ^{3}[Ru(bpy)$_3$]$^{2+}$, which results in the "energy reservoir" effect (case of O$_2$-free solvent), or deactivated via diffusion-controlled quenching (case of air-equilibrated solvent). Thus, in this model study we have been able to fully disentangle the antenna and reservoir effects of two different types of energy transfer mechanisms, which are singlet—singlet and triplet—triplet in terms of their electronic nature.

IC025811D

(50) Closs, G. H.; Johnson, M. D.; Miller, J. R.; Piotrowiak, P. *J. Am. Chem. Soc.* **1989**, *111*, 3751.
(51) McConnell, H. *J. Chem. Phys.* **1961**, *35*, 508.
(52) Newton, M. D.; Sutin, N. *Annu. Rev. Phys. Chem.* **1984**, *35*, 437.
(53) Scandola, F.; Argazzi, R.; Bignozzi, C. A.; Indelli, M. T. *J. Photochem. Photobiol. A, Chem.* **1994**, *82*, 191.